Ferromagnetic transition and specific heat of $Pr_{0.6}Sr_{0.4}MnO_3$

S. Rößler,[1,*] Harikrishnan S. Nair,[2] U. K. Rößler,[3] C. M. N. Kumar,[2] Suja Elizabeth,[4] and S. Wirth[1]

[1]*Max Planck Institute for Chemical Physics of Solids, Nöthnitzer Straße 40, D-01187 Dresden, Germany*

[2]*Jülich Centre for Neutron Sciences-2, Peter Grünberg Institute-4, Forschungszentrum Jülich GmbH, D-52425 Jülich, Germany*

[3]*IFW Dresden, Postfach 270016, D-01171 Dresden, Germany*

[4]*Department of Physics, C.V. Raman Avenue, Indian Institute of Science, Bangalore-560012, India*

(Received 30 June 2011; revised manuscript received 20 October 2011; published 16 November 2011)

The critical properties of orthorhombic $Pr_{0.6}Sr_{0.4}MnO_3$ single crystals were investigated by a series of static magnetization measurements along the three different crystallographic axes as well as by specific heat measurements. A careful range-of-fitting-analysis of the magnetization and susceptibility data obtained from the modified Arrott plots shows that $Pr_{0.6}Sr_{0.4}MnO_3$ has a very narrow critical regime. Nevertheless, the system belongs to the three-dimensional (3D) Heisenberg universality class with short-range exchange. The critical exponents obey Widom scaling and are in excellent agreement with the single scaling equation of state $M(H,\epsilon) = |\epsilon|^{\beta} f_{\pm}(H/|\epsilon|^{(\beta+\gamma)})$; with f_+ for $T > T_c$ and f_- for $T < T_c$. A detailed analysis of the specific heat that account for all relevant contributions allows us to extract and analyze the contribution related to the magnetic phase transition. The specific heat indicates the presence of a linear electronic term at low temperatures and a prominent contribution from crystal field excitations of Pr. A comparison with data from literature for $PrMnO_3$ shows that a Pr-Mn magnetic exchange is responsible for a sizable shift in the lowest lying excitation.

DOI: 10.1103/PhysRevB.84.184422 PACS number(s): 75.47.Lx, 75.40.Cx

I. INTRODUCTION

Colossal magnetoresistive (CMR) oxides of the manganite family with the generic formula $R_{1-x}A_xMnO_3$ (R = rare earth ion, A = alkaline earth or equivalent ion) possess a complex phase diagram that often includes charge order (CO)/orbital order (OO), metal-insulator (MI) transitions, and various magnetic phases tunable as a function of composition, magnetic field and/or temperature.[1–3] The physical properties of these materials strongly depend on subtle structural distortions. The composition $Pr_{0.6}Sr_{0.4}MnO_3$, which forms the subject of this paper, has been reported to constitute a ferromagnet with a Curie temperature $T_C \sim 297$ K.[4] $Pr_{0.6}Sr_{0.4}MnO_3$ also undergoes a structural phase transition from a high-temperature orthorhombic $Pnma$ to a low-temperature monoclinic $I2/a$ space group which was reported to take place at $T_{str} \sim 100$ K.[5] Powder neutron diffraction studies report structural phase separation below T_{str}.[5] Furthermore, the magnetization curves (M-H) measured below the structural transition temperature are found to be anomalous: The virgin curve stays outside the subsequent M-H hysteresis loops[6] thereby suggesting that the structural phase separation has a profound influence on the magnetic properties. Optical conductivity data[7] on $Pr_{0.6}Sr_{0.4}MnO_3$ in applied magnetic field deviate from the expected universal scaling. In particular, a nearly linear $|M|$ dependence of the magneto-optical conductivity in the critical regime indicates strong ferromagnetic spin fluctuations of Mn above T_C.[7] The irreversible magnetization processes related to the structural phase separation and the anomalous behavior of the magneto-optical conductivity motivated us to investigate some basic physical properties of $Pr_{0.6}Sr_{0.4}MnO_3$ single crystals in order to unambiguously distinguish between conventional and unconventional properties of this essentially metallic and ferromagnetic mixed-valent manganite. The main focus is the nature of the paramagnetic (PM)-ferromagnetic (FM) transition. Hence we present a scaling analysis of static magnetization data supplemented by a detailed analysis of the specific heat C_p within the temperature range 2–350 K, that covers both the PM-FM transition and the structural transitions.

The critical nature of manganites near a PM-FM phase transition have been the subject of many studies.[8–25] Different experimental techniques have been used in these investigations to obtain the critical exponent β of the spontaneous magnetization. The values of the exponent from these reports were found in a range from 0.3 to 0.5 which covers the mean-field value ($\beta = 0.5$) as well as the values corresponding to the three-dimensional (3D) isotropic Heisenberg ($\beta = 0.365$) and the 3D Ising ($\beta = 0.325$) universality classes. In addition to the above variety of continuous phase transitions, first-order nature of the PM-FM transition was found in in the case of $LaMnO_{3.14}$[13] and $La_{0.7}Ca_{0.3}MnO_3$.[26] The first-order phase transition has been recently found in the phase diagrams generated by large-scale Monte Carlo simulations within the two-orbital model Hamiltonian.[27] This suggests that the PM-FM transitions in manganites display different properties varying from continuous transitions due to short-range exchange to first-order transitions.

Although our preliminary investigations[6] of the resistivity at the paramagnetic-ferromagnetic (PM-FM) transition in $Pr_{0.6}Sr_{0.4}MnO_3$ already suggested that the critical exponents most probably belong to the class of conventional isotropic ferromagnets, a clear-cut evidence from the magnetization data was missing. Therefore, we here report a detailed analysis of magnetization. The results reveal that the modified Arrott plots provide straight lines for a range of exponents β and γ (see definition below), including those belonging to both the three-dimensional (3D) Heisenberg as well as 3D Ising universality classes. These observations suggested a possible role of anisotropy affecting the asymptotic critical properties. Furthermore, a very recent investigation[28] of critical behavior in polycrystalline $Pr_{0.55}Sr_{0.45}MnO_3$ by Fan *et al.* using the field dependence of magnetic entropy change reports exponents close to the mean-field values. In their method, only two

of the critical exponents, magnetic entropy change n, and that of the magnetic isotherm δ, were experimentally determined. From these values of n and δ, values of the interrelated β and γ were numerically computed. However, for a more stringent test, it is required to independently obtain at least three of the exponents. Moreover, in the polycrystalline samples, the effect of anisotropy is averaged out and thus concealing some of the physics we are interested in. In order to clarify these issues, we performed additional magnetization measurements along all three orthorhombic crystallographic axes of our single crystal in the critical regime. All our measurements indicate that even though the magnetic properties of this material are fairly complex, it can be classified as a conventional ferromagnetic metal. Furthermore, we show that the magnetic anisotropy is not strong enough to reveal the expected crossover toward the scaling of the 3D Ising universality class. The analysis of the critical properties is supplemented by investigations of the specific heat in the temperature range 2–350 K which evidences metallic and ferromagnetic properties. In addition to that, an appreciable contributions from excitations of the crystalline electric field (CEF) split levels of the Pr^{3+} ions are observed, which allows us to estimate for the Pr-Mn magnetic exchange in this system.

II. METHODS

A. Experiments

The samples used in the present study were single crystals of $Pr_{0.6}Sr_{0.4}MnO_3$ grown by the optical floating zone method. The crystals were prepared from high purity precursors Pr_6O_{11}, $SrCO_3$ and MnO_2. The single-crystalline quality of the samples was confirmed by Laue photography, and the chemical composition was ascertained by inductively coupled plasma atomic emission spectroscopy using a Perkin Elmer Optima 2000 spectrometer. The phase purity of the crystals was verified by powder x-ray diffraction (XRD) with Cu $K\alpha$ radiation on pulverized pieces from these crystals. A cuboidal sample of dimension $2 \times 2 \times 2$ mm^3 was extracted from the boule, oriented, and used in further experiments. The field cooled (FC) and zero-field cooled (ZFC) magnetization protocols, and the magnetization isotherms for the critical analysis in the temperature range 290–311 K in steps of 0.5 K (and, where required, 0.25 K) were measured using a SQUID (Quantum Design) magnetometer. Specific heat was measured by means of a commercial physical property measurement system (Quantum Design).

B. Critical analysis

According to the scaling hypothesis, the critical properties of a magnetic system that undergoes a continuous phase transition can be characterized by a set of interrelated critical exponents α, β, γ, and δ.[29] Here α is the specific heat (C_p) exponent, and the exponents β and γ are derived from spontaneous magnetization (M_s) below the transition temperature T_C and initial susceptibility (χ_0) above T_C, respectively. The exponent δ describes the behavior of the magnetization M in an applied field H at T_C. Thus, the singular components of the physical properties depend on the reduced temperature $\epsilon = (T - T_C)/T_C$ as follows:

$$C_p \sim A^{\pm}|\epsilon|^{-\alpha}. \quad (1)$$

Here A^+ is critical amplitude for $T > T_C$ and A^- is the corresponding one for $T < T_C$:

$$M_s(T) \sim M_0|\epsilon|^{\beta}, \quad \epsilon < 0\ (H \to 0). \quad (2)$$

$$\chi_0(T)^{-1} \sim (h_0/M_0)\epsilon^{\gamma}, \quad \epsilon > 0. \quad (3)$$

$$M \sim DH^{1/\delta}, \quad \epsilon = 0, \quad (4)$$

where M_0, h_0/M_0, and D are critical amplitudes.

The magnetic equation of state in the critical region is given by

$$M(H,\epsilon) = |\epsilon|^{\beta} f_{\pm}(H/|\epsilon|^{\beta+\gamma}), \quad (5)$$

where f_+ for $T > T_C$ and f_- for $T < T_C$ are regular analytic functions. Thus, two universal curves are expected from Eq. (5), one for temperatures above T_C and another one for temperatures below T_C. The experimental verification of the existence of these two universal curves are usually taken as a stringent test for proper scaling.

III. RESULTS

A. Crystal structure

The Rietveld method[30] as implemented in the Fullprof code[31] was used for the refinement of the powder XRD data.

The experimentally observed diffraction intensities I_{obs} along with the calculated intensities (refinement) I_{calc}, their difference $I_{obs} - I_{calc}$, and the Bragg positions are presented in Fig. 1. The crystal structure was refined within the *Pnma* space group with the lattice parameters $a = 5.4859(1)$ Å, $b = 7.6790(1)$ Å, and $c = 5.4443(9)$ Å. The lattice parameters are consistent with the crystal structure of $Pr_{0.6}Sr_{0.4}MnO_3$ reported earlier from x ray as well as neutron powder diffraction.[4,5,32]

B. Magnetization

The static magnetization curves of $Pr_{0.6}Sr_{0.4}MnO_3$ measured in a zero-field cooled and field cooled state in an applied magnetic field of 100 Oe parallel to crystallographic

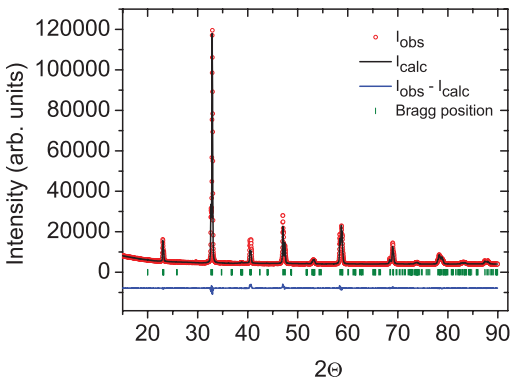

FIG. 1. (Color online) The powder x-ray diffractogram of $Pr_{0.6}Sr_{0.4}MnO_3$ showing the observed, calculated, and difference intensities along with the Bragg positions.

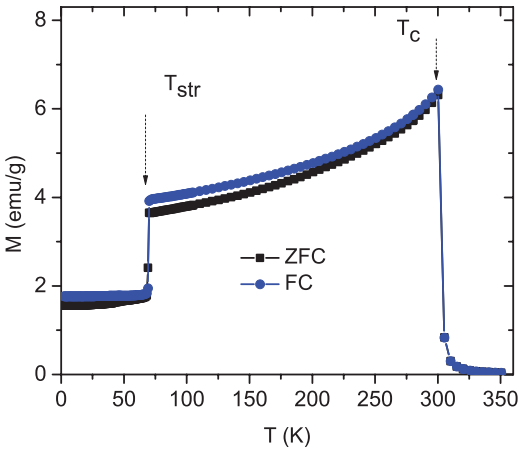

FIG. 2. (Color online) The temperature dependence of dc magnetization measured in a zero-field cooled (ZFC) and field cooled (FC) state in a magnetic field of 100 Oe applied parallel to the crystallographic a axis. T_C and T_{str} mark the ferromagnetic and structural transitions, respectively.

a axis are presented in Fig. 2. Two transitions are evident: a high-temperature transition at $T_C \approx 300$ K which signals the ferromagnetic transition, and a second one, which marks the structural transition at $T_{str} \approx 65$ K from the orthorhombic $Pnma$ to the monoclinic $I2/a$ space group.[5] The critical properties of $Pr_{0.6}Sr_{0.4}MnO_3$ were analyzed from the static magnetization data. First we discuss the analysis of the magnetization data measured along the crystallographic a axis. The M-H isotherms are presented in Fig. 3. The inset

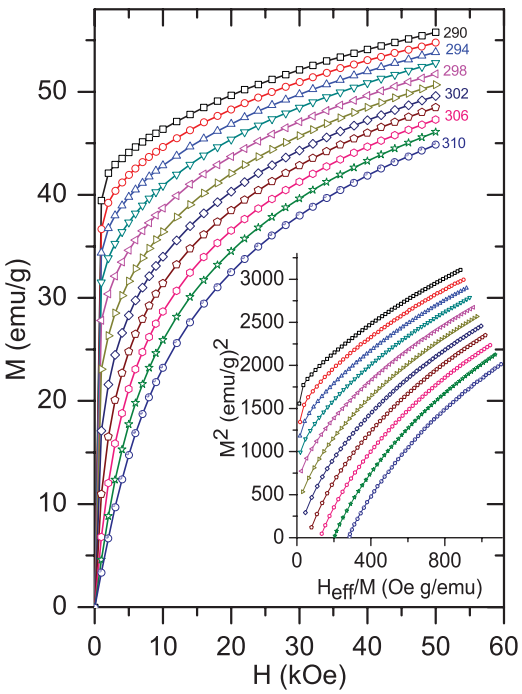

FIG. 3. (Color online) Magnetization isotherms for $Pr_{0.6}Sr_{0.4}MnO_3$ along the crystallographic a axis from 0 up to 5 T in the temperature range 290–311 K covering T_C. Only selected data are shown for clarity. The inset displays Arrott plots in the same range of magnetic field and temperature.

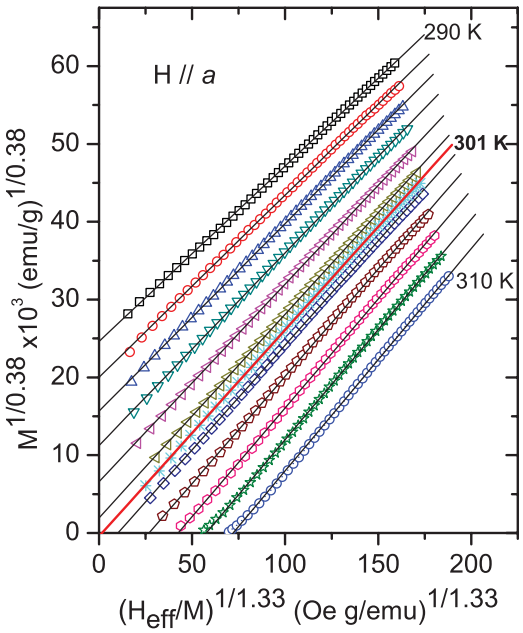

FIG. 4. (Color online) Modified Arrott plot for $Pr_{0.6}Sr_{0.4}MnO_3$ with optimized trial values of $\beta = 0.38$ and $\gamma = 1.33$. The isotherm at $T = 301$ K passing through the origin gives an estimate for the Curie temperature T_C.

presents Arrott plots M^2 vs $H_{\rm eff}/M$, where $H_{\rm eff}$ is the effective magnetic field after correcting for demagnetization effects. Obviously the Arrott plots in the present case are highly nonlinear and, hence, do not obey the mean-field theory of phase transitions, that is, for $\beta = 0.5$ and $\gamma = 1$. Therefore, modified Arrott plots were constructed in which $M^{1/\beta}$ was plotted against $(H_{\rm eff}/M)^{1/\gamma}$. For the trial values $\beta = 0.38$ and $\gamma = 1.33$ an excellent plot was obtained: It can clearly be seen from Fig. 4 that the curves within this modified Arrott plots exhibit remarkably linear behavior at all measured temperatures with the straight line at $T = 301$ K passing very close through the origin. We note that a linear behavior in the modified Arrott plots was also observed with the trial values of $\beta = 0.32$ and $\gamma = 1.24$, yet the former values gave a better quality of the linear fits. Therefore, the linear plots in Fig. 4 with the trial values of $\beta = 0.38$ and $\gamma = 1.33$ were extrapolated to the abscissa and the ordinate to obtain the values of spontaneous magnetization $M_s(T,0)$ and inverse susceptibility χ_0^{-1}, respectively. The resulting data of $M_s(T,0)$ and χ_0^{-1} as a function of temperature are summarized in Fig. 5. A power-law fit to this plot following Eq. (2) yields the values of $\beta = 0.365(4)$ and $T_C = 301.3(2)$ K. A similar analysis of the inverse susceptibility following Eq. (3) gives the values $\gamma = 1.309(3)$ and $T_C = 301.2(2)$ K. These values of β and γ are close to our starting values. The critical exponent $\delta = 4.648(4)$ was obtained directly from the critical isotherm at 301 K following Eq. (4) (Fig. 6). On the other hand, the Widom scaling equation[33,34] predicts

$$\delta = 1 + \gamma/\beta. \tag{6}$$

Using the values of β and γ obtained from the fits, we get $\delta = 4.586$ from Eq. (6) which is very close to the directly determined value from the critical isotherm and thus supports

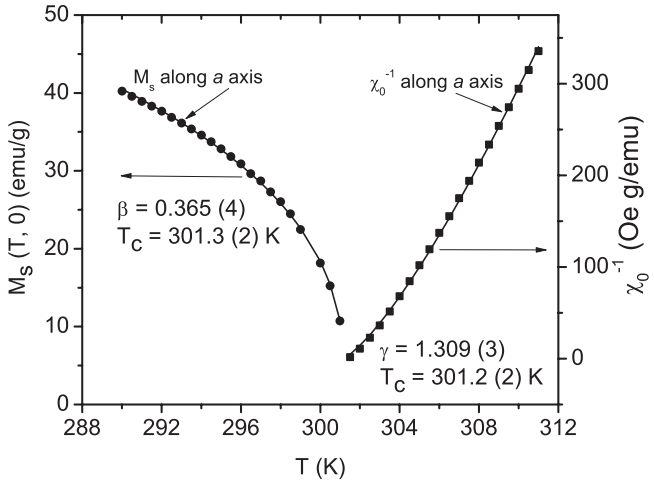

FIG. 5. Spontaneous magnetization (left) and initial susceptibility (right) vs temperature of $Pr_{0.6}Sr_{0.4}MnO_3$ as obtained from our modified Arrott plot. The solid lines represent power-law fits, as explained in the text.

the scaling. In order to verify whether the data obey the magnetic equation of state [Eq. (5)] we plot $M|\epsilon|^{-\beta}$ as a function of $H|\epsilon|^{-(\beta+\gamma)}$ in Fig. 7. A double-logarithmic plot of the same data is presented in the inset. All data in the temperature range $295 \leqslant T \leqslant 308$, corresponding to a reduced temperature interval $|\epsilon| \leqslant 0.025$, collapse perfectly into two universal curves, one for $T < T_C$ and another for $T > T_C$. Thus, the obtained critical exponents agree well with the prediction of the scaling hypothesis. The experimentally determined values of the exponents $\beta = 0.365(4)$, $\gamma = 1.309(3)$, and $\delta = 4.6483(4)$ are close to the expected critical exponents for the Heisenberg universality class, $\beta_H = 0.368$, $\gamma_H = 1.396$, and $\delta_H = 4.783$.[35] But on a closer look, the value of the exponent γ appears to be quite low compared to the theoretical γ_H. This prompted us to conduct a similar analysis of the magnetization data along the crystallographic b and c axes. Again, from the modified Arrott plots (similar to the one presented in Fig. 4) M_s and χ_0^{-1} values were extracted.

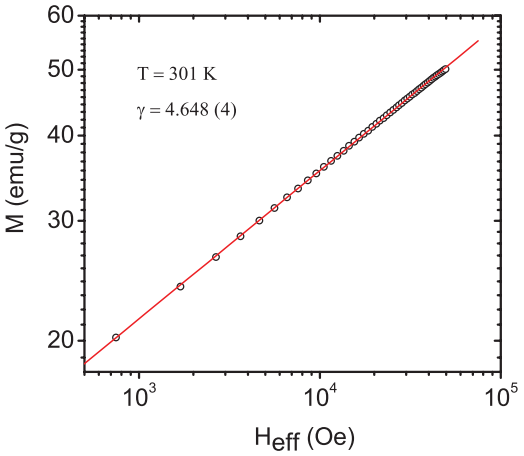

FIG. 6. (Color online) M along a axis in dependence on $H_{\rm eff}$ plotted for $T = 301$ K. The straight line is the linear fit following Eq. (4). Here H is replaced by $H_{\rm eff}$ to account for demagnetization effects.

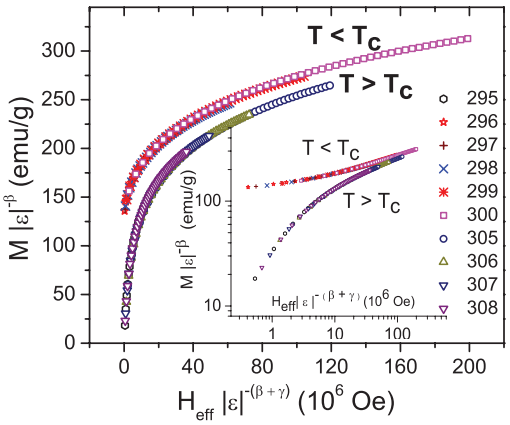

FIG. 7. (Color online) Scaling plots following the magnetic equation of state for $Pr_{0.6}Sr_{0.4}MnO_3$. Measurements were done with magnetic field along a axis. Clearly two universal curves above and below T_c are obtained. The inset plots the same data in a double logarithmic presentation.

These data are plotted in Fig. 8. A power-law fit according to the Eq. (2) to the magnetization data yielded $T_C = 300.30(4)$ K and $\beta = 0.344(4)$ for b axis and $T_C = 302.10(2)$ K and $\beta = 0.364(3)$ for c axis. The values of the exponent β were found to be insensitive to the temperature range of fitting, but those of the exponent γ did depend on the range of fitting. Stable values of the exponents were obtained for χ_0^{-1} data along the b and c axis for the range $5.32 \times 10^{-4} \leqslant |\epsilon| \leqslant 0.012$ and $1.6 \times 10^{-3} \leqslant |\epsilon| \leqslant 0.016$, respectively. From a power-law fit to Eq. (3) we obtained $T_c = 300.2(2)$ K; $\gamma = 1.34(7)$ for b axis and $T_c = 302.0(2)$ K; $\gamma = 1.34(9)$ for c axis. These values also satisfy the scaling equation of state. There is an obvious anisotropy of the critical temperatures determined along different directions. This effect is expected owing to an anisotropy of the magnetic system, which may be associated, for example, to the rare-earth magnetism of Pr in this system. Our scaling analysis, by extrapolating from high fields, determines the properties of critical fluctuations for the leading couplings in the magnetic system and suppresses the secondary

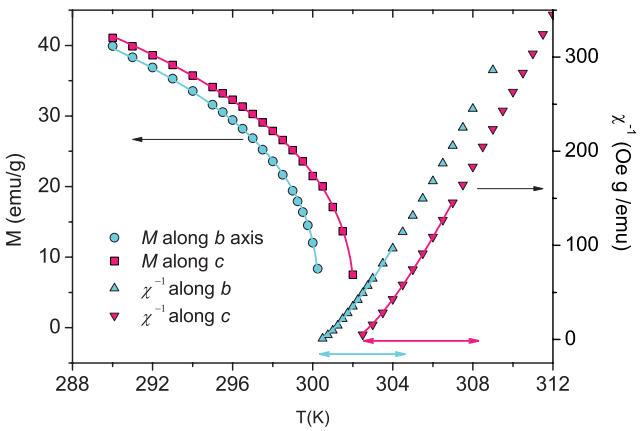

FIG. 8. (Color online) Spontaneous magnetization (left) and initial susceptibility (right) vs temperature of $Pr_{0.6}Sr_{0.4}MnO_3$ along the crystallographic b and c axes. The solid lines represent power-law fits, as explained in the text. The horizontal arrows close to the x axis indicate the T range used for the fit above T_c.

effects of anisotropies or dipolar couplings. A determination of the crossover behavior, for example, toward the expected behavior of a 3D Ising system was inconclusive, which is also expected as there is a clear hierarchy of magnetic couplings with the exchange being much larger than any magnetic anisotropic couplings. Thus, anisotropy effects are only seen in the nonuniversal values of the critical temperatures, according to our scaling analysis. The observation of this anisotropy, however, indicates that scaling analysis using measurements in zero, or low, fields may lead to substantial artifacts as they may display fluctuation properties in the crossover regimes toward anisotropic couplings without reaching an asymptotic or effective scaling behavior. The phase separation below 65 K due to the first-order structural transition does not affect the ferromagnetic transition at high temperature. The results show that the magnetization can be effectively used as an order parameter for the high temperature phase transition. Thus, our analysis demonstrates that the present system $Pr_{0.6}Sr_{0.4}MnO_3$ displays a conventional continuous PM-FM phase transition and can nicely be compared to the one in $Nd_{0.6}Pb_{0.4}MnO_3$[14] or $Pr_{1-x}Pb_xMnO_3$[17] within the class of mixed-valent ferromagnetic manganites, as well as to Ni.[36] Our results can be generalized to the manganite systems that have high ferromagnetic transition temperatures and are far away from a charge-ordered antiferromagnetic phase. Theoretical work on the manganites has focused on the formation of nanoscale inhomogeneities, caused by the formation of correlated magnetic polarons, and electronic phase separation in order to explain the colossal effects in transport.[2] At a continuous magnetic ordering transition, universality guarantees that the critical properties should only depend on the order parameter symmetry, dimensionality, and range of interactions independent of microscopic details. The existence of magnetic polaronic entities introduces an additional microscopic length scale, but it is not expected to influence the critical properties. Therefore, the finding of a continuous phase transition in $Pr_{0.6}Sr_{0.4}MnO_3$ does not *per se* contradict microscopic models involving correlated magnetic polarons. However, couplings of the magnetic subsystem to other fluctuating modes under the influence of disorder may cause another type of magnetic ordering transitions. For example, Monte Carlo simulations performed for realistic models of manganites[27,37] predict short-range correlations among polarons in the paramagnetic state, but also the occurrence of first-order phase transitions in the pure case without quenched disorder. These models[27,37] are mainly focused on the manganites close to a bicritical point in the temperature-composition phase diagram. Such systems could display unconventional types of continuous magnetic ordering transitions if the magnetic order is a secondary order parameter driven by a structural or orbital ordering. In particular, strong quenched disorder could lead to a rounded continuous phase transition ruled by a universality class for disordered systems with a different kind of order-parameter symmetry. Theoretically, corresponding finite-temperature critical properties have not been investigated in detail yet for the manganites. However, the finding of a continuous and conventional magnetic ordering transition in $Pr_{0.6}Sr_{0.4}MnO_3$ with relatively high $T_C \sim 300$ K shows that this system is far from such a behavior at a bicritical point.[38]

C. Specific heat

The specific heat of $Pr_{0.6}Sr_{0.4}MnO_3$ is presented in Fig. 9(a) (black open squares). The PM-FM transition is obvious in the specific heat as a peak around 300 K. The structural transition is discernible as a small step at $T_{str} \simeq 68.5$ K [Fig. 9(b)]. Our single crystal data are broadly comparable to specific heat data in the temperature range from 2 to 300 K for polycrystalline $Pr_{0.6}Sr_{0.4}MnO_3$ material presented by Lees *et al.*[39] Although the anomaly associated with the structural transition in their data appears as a broad shoulder between 75 and 100 K with a maximum at about 88 K, the magnetic transition seems to take place above 300 K in these data. These deviations may be due to slight differences in stoichiometry as well as due to the differences in the properties between polycrystalline materials and single crystals, as observed, for example, also in specific heat data for different samples of $Pr_{0.63}Ca_{0.37}MnO_3$.[40]

We now analyze the specific heat data for our single crystal by considering all possible contributions that are known to occur in rare-earth-based mixed-valent manganites. These are contributions from the lattice ($C_{\rm latt}$), electronic contributions due to the metallic character of $Pr_{0.6}Sr_{0.4}MnO_3$ ($C_{\rm el}$), magnetic contributions ($C_{\rm mag}$), Schottky-like anomalies from the CEF levels of the Pr^{3+} (C_S), and magnetic hyperfine-field excitations of the ^{55}Mn nuclei ($C_{\rm hyp}$):

$$C_p = C_{\rm latt} + C_{\rm el} + C_{\rm mag} + C_S + C_{\rm hyp}. \quad (7)$$

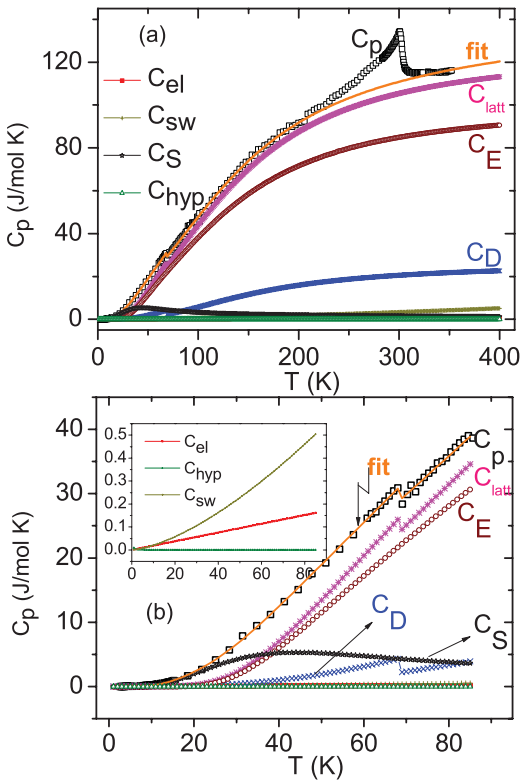

FIG. 9. (Color online) (a) The specific heat of $Pr_{0.6}Sr_{0.4}MnO_3$ plotted along with the relevant fit lines pertaining to the model described in the text. The different contributions to the lattice part are also plotted separately. (b) The same data set at low temperatures. In the inset, for clarity in an enlarged scale the contributions from the $C_{\rm el}$, $C_{\rm hyp}$, and $C_{\rm sw}$ are presented.

The magnetic contributions stemming essentially from the ferromagnetic order of the Mn subsystem may be split into a low-temperature part due to spin waves in the ferromagnetic state and an excess contribution due to the magnetic ordering near T_C,

$$C_{\mathrm{mag}} = C_{\mathrm{sw}} + C_{\mathrm{exc}}. \tag{8}$$

In these considerations, contributions from a separate ordering of magnetic moments on the Pr sublattice are neglected, because there is no evidence of Pr contributing to the ordered magnetic moment at T_C. Moreover, it is assumed that the structural transition is a first-order transition so that any related anomalies in the specific heat are δ-like and confined to a narrow temperature region around T_{str}.

Obviously, it is not possible to derive the numerous parameters of the specific heat model Eq. (7) from the measured data in a straightforward fitting exercise. Furthermore, it turns out that major contributions overlap over most of the temperature range such that there is no satisfactory way to separate them out. Instead, we model the specific heat by including circumstantial information to fix certain contributions. This will allow us to derive estimates for the remaining contributions in the temperature range outside of the anomaly associated to the magnetic ordering at T_C.

At low temperatures the electronic contribution C_{el}, and the spin-wave contribution C_{sw},

$$C_{\mathrm{el}} = \gamma_1 T, \tag{9}$$

$$C_{\mathrm{sw}} = B_{3/2}\, T^{3/2}, \tag{10}$$

due to ferromagnetic order dominate. Generally, it is difficult to separate these two similar power laws even for common metallic ferromagnets. Moreover, we find that the Schottky-like anomaly from the lowest CEF level appreciably contributes already above 8 K. This precludes a quantitative distinction between C_{el} and C_{sw}. At lowest temperatures, between 2 and 3 K, a nuclear hyperfine field contribution C_{hyp},

$$C_{\mathrm{hyp}} = \alpha_{-2}/T^2 \tag{11}$$

is discernible, in agreement with earlier studies on mixed-valent manganites.[39,42] This contribution is related to the magnetic influence of the electronic Mn spins on the ^{55}Mn nuclei. In our model, we adopt $\alpha_{-2} \simeq 9$ mJ K/mol obtained by Woodfield *et al.*[42] for $La_{1-x}Sr_xMnO_3$ with $0.0 \leqslant x \leqslant 0.3$ under the assumption that the hyperfine fields at the Mn-nuclear sites are similar in both metallic and ferromagnetic materials $La_{1-x}Sr_xMnO_3$ and $Pr_{1-x}Sr_xMnO_3$.

Similarly, we fix the spin wave contribution C_{sw} by data from other studies. From inelastic neutron scattering, the spin-wave dispersion and the stiffness D_{sw} have been determined for $Pr_{0.625}Sr_{0.375}MnO_3$.[43,44] These data show that the low-lying spin waves are well described by the dispersion of a simple cubic ferromagnet, with nearest-neighbor coupling and a negligible spin-wave gap. Hence, we fix the spin-wave contribution to the specific heat [Eq. (10)] by the appropriate expression for a simple cubic ferromagnet with nearest-neighbor exchange[45]

$$\begin{aligned} B_{3/2} &= \frac{R\,V_{\mathrm{cell}}}{4\pi^2}\left(\frac{\mathrm{k_B}}{D_{\mathrm{sw}}}\right)^{3/2}\int_0^\infty \frac{x^{5/2}e^x}{(e^x-1)^2}\,dx \\ &= 4.45823\,\frac{R\,V_{\mathrm{cell}}}{4\pi^2}\left(\frac{\mathrm{k_B}}{D_{\mathrm{sw}}}\right)^{3/2} \\ &\approx 0.60\ \mathrm{mJ/(mol\,K^{5/2})}, \end{aligned} \tag{12}$$

where R is the ideal gas constant, $V_{\mathrm{cell}} = 57.34$ Å^3 the volume per formula unit, and $\mathrm{k_B}$ is Boltzmann constant. The spin-wave stiffness was taken from Refs. 43 and 44 as $D_{\mathrm{sw}} = 165$ meV Å^2 $= 1915\ k_{\mathrm{B}}$ K Å^2.

All relevant contributions for the low temperature range result in

$$C_p(T) = \alpha_{-2}/T^2 + B_{3/2}T^{3/2} + \gamma_1\, T + B_3 T^3, \tag{13}$$

where the first two contributions have already been accounted for. The parameters γ_1 and B_3 for the remaining electronic and the leading-order lattice contribution, respectively, are determined by plotting $C_p(T)/T - \alpha_{-2}/T^3 - B_{3/2}T^{1/2}$ versus T^2 (Fig. 10). For the temperature range $2 < T < 8$ K, a linear fit gives $\gamma_1 = 1.8(4)$ mJ/(mol K^2) and $B_3 = 2.1(1)$ mJ/(mol K^4). The parameter γ_1 corresponds to a density of states at the Fermi level, $N(\epsilon_F) = 3\gamma_1/(\pi^2\,\mathrm{k_B}^2) = 1.3 \times 10^{22}$ eV^{-1} cm^{-3}, which is a reasonable value similar to the one reported for $La_{1-x}Sr_xMnO_3$,[42] and in fair agreement with band structure calculations for $La_{1-x}Ca_xMnO_3$.[46] Alternatively, we attempted to fit the low temperature specific heat data directly to Eq. (13), with four parameters. These fits were not proper and failed to provide any reliable values because of their correlations.

For higher temperatures the Schottky-like anomalies due to CEF levels and the lattice contribution dominate the specific heat. The presence of CEF level excitations within the thermally activated energy range is well established in Pr-based perovskites from inelastic neutron scattering studies on $PrGaO_3$[47] and $PrNiO_3$.[48] Specific heat data for $PrGaO_3$ corroborate the presence of CEF level excitations.[49] It should be noted in this respect that specific heat data of doped Pr-based manganites $Pr_{1-x}Ca_xMnO_3$,[40,50] $Pr_{1-x}Ca_x(Mn,Al)O_3$,[51] or $Pr_{1-x}Sr_xMnO_3$,[39,51] did not exhibit any sign of peak-like anomalies. Moreover, these previously reported data were

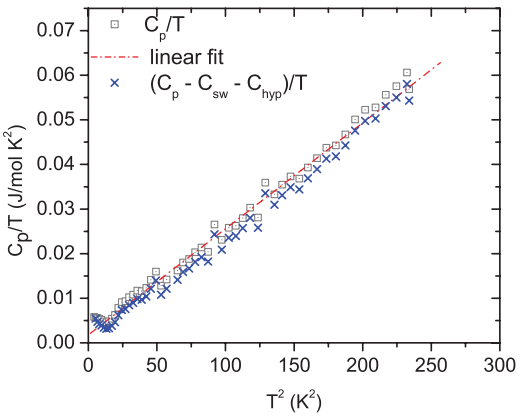

FIG. 10. (Color online) C_p/T vs T^2 plot and linear fit for the estimation of electronic and lattice terms γ_1 and B_3.

TABLE I. Crystal field level excitations $\Delta_i^{(0)}$ (in K) for $PrMnO_3$ from Ref. 41, levels for $i \geqslant 3$ are used as fixed input in the fitting of specific heat data.

i	0	1	2	3	4	5	6	7	8
$\Delta_i^{(0)}$ (K)	0	17	75	148	188	377	435	731	1023

analyzed without taking into account effects from CEF level excitations.[39,40,51] In contrast, a detailed investigation of the specific heat in external magnetic fields for the mixed-valent, ferromagnetic, and insulating manganite $Pr_{0.8}Ca_{0.2}MnO_3$ suggests the presence of a Schottky-like contribution at low temperatures.[52] In undoped antiferromagnetic $PrMnO_3$, specific heat data reveal a clear Schottky-like peak anomaly at about 8–9 K.[53,54] This peak shifts to higher temperatures in magnetic fields.[54] From infrared transmission studies, Jandl *et al.*[41] determined low-lying energy levels at 13 and 120 cm^{-1} and derived a set of crystal-field parameters for $PrMnO_3$ to calculate a full set of levels for the $^3H_4$ ground-state multiplet in the range between 19 and 1000 K. These results are essentially consistent with the analysis of specific heat data in magnetic field by Cheng *et al.*[54] They also suggest that a molecular field of exchange origin H_{ex} leads to a strong upward shift of the lowest excited CEF levels in Pr. In our model, the CEF level excitations are included by evaluating the specific heat from the partition sum $Z_S = \sum_i \exp[-\Delta_i/T]$, $i = 0, \ldots, 8$ that is attributed to the nine levels Δ_i of the Pr $^3H_4$ ground-state multiplet split by the crystal electric field. This gives a Schottky-like contribution to the partially occupied rare-earth sublattice,

$$C_S = \frac{(1-x)R}{T^2}\left\{\left[\frac{\Sigma_i \Delta_i^2 \exp(-\Delta_i/T)}{Z_S}\right] - \left[\frac{\Sigma_i \Delta_i \exp(-\Delta_i/T)}{Z_S}\right]^2\right\}. \quad (14)$$

In the fit we only use the first excitation energies of the two excited levels ($i = 1, 2$) as fit parameters, and fix the remaining levels $\Delta_i^{(0)}$, $i = 3, \ldots, 8$, at the energy differences of the levels determined from the crystal field parametrization for $PrMnO_3$ by Jandl *et al.*,[41] as listed in Table I. The exact values of the higher levels are not important, as they only provide a relatively small and very broad background to the fit. In our model, the higher levels were only introduced for conceptual and quantitative consistency.

The lattice contribution is described by a weighted sum of Debye and Einstein mode contributions,

$$\begin{aligned} C_{\text{latt}}(T) &= C_D + C_E, \\ [0.1\text{ cm}] &= 3\,R\,r\left(3w_D\left(\frac{T}{\theta_D}\right)^3\int_0^{\theta_D/T}\frac{\eta^4 e^\eta}{(e^\eta-1)^2}\,d\eta \right. \\ &\quad + (1-w_D)\left\{\frac{(1-w_1)\exp\left(\theta_E^{(1)}/T\right)}{\left[\exp\left(\theta_E^{(1)}/T\right)-1\right]^2}\left(\frac{\theta_E^{(1)}}{T}\right)^2\right. \\ &\quad \left.\left. + \sum_k^{N_E} w_{k-1}\frac{\exp\left(\theta_E^{(k)}/T\right)}{\left[\exp\left(\theta_E^{(k)}/T\right)-1\right]^2}\left(\frac{\theta_E^{(k)}}{T}\right)^2\right\}\right), \end{aligned} \quad (15)$$

where r is the number of atoms per formula unit. The free fitting parameters are the Debye temperature θ_D, the Einstein mode temperatures $\theta_E^{(k)}$, and the respective weights w_D, w_k. The lattice model has to be refined in order to consider the structural transition at $T_{str} = 68.5$ K. We assume that the acoustic, that is, elastic lattice phonons are most affected by the structural transition and that the influence of the structural transition on all other contributions to the specific heat are negligible. Therefore, two different Debye temperatures θ_D^{LT} and θ_D^{HT} are used for the fit in the two temperature ranges $T < T_{str}$ and $T > T_{str}$, respectively. The other parameters, including the weights in Eq. (15), are kept as unique fitting parameters and adjusted globally in the whole temperature range considered. For the final fit, data from the temperature ranges $2 \leqslant T \leqslant 185$ K and $345 < T < 355$ K have been chosen, thus excluding a wide range of data around T_C. Checks on the range of fitting show that within these limits fits are stable. Only two Einstein modes $N_E = 2$ suffice to represent the optical phonons; attempts to use more Einstein modes do not lead to improved fits. The data and the fit are shown in Fig. 9, and the derived parameters are collected in Table II. The model reproduce the overall data rather well. It is satisfactory that the weight of the Debye-like elastic contributions yields $w_D \simeq 0.2$, which appears to be a good estimate for acoustic phonon contributions in the perovskite structure. The determined Debye temperatures $\theta_D = 504$ and 656 K are much larger than values around 300 K often reported for perovskite manganites.[39,42,55,56] Reasons for this discrepancy are obvious: the present model is based on (i) a composite phonon density of states including low-lying Einstein modes. Hence there is no reason to expect similar values for the Debye temperatures. (ii) The fit includes high temperature data while low Debye temperatures are usually obtained from fits to low temperature data.

The most prominent result of our fit procedure is the presence of a sizable contribution C_S from the CEF level excitations. It is not possible to fit more than the first two excited CEF levels Δ_1 and Δ_2 and retain a stable fit. These two levels are shifted to higher temperatures compared to the Schottky-like peak observed in antiferromagnetic $PrMnO_3$.[53,54] In fact, C_S dominates the specific heat for temperatures $10 \leqslant T \leqslant 30$ K, but the contributions are concealed by the simultaneous rise of the lattice specific heat C_{latt} [Fig. 9(b)]. A comparison to the specific heat data for $La_{0.7}Sr_{0.3}MnO_3$ from Ref. 42, as a related metallic and ferromagnetic manganite without electronic contributions from rare-earth ions, indeed shows that our experimental data are significantly enhanced already at 10 K. The shifted value for the first excited CEF level Δ_2 from our fits (Table II) as compared to the level for $PrMnO_3$ from Ref. 41 in Table I can be used to estimate the molecular field at the Pr site, which is described

TABLE II. Parameters for the specific heat model of Eq. (7) for the global fit to experimental data excluding the temperature range $185 \leqslant T \leqslant 345$, as shown in Fig. 9. Parameters with an asterisk $*$ have been fixed prior to the fit, crystal field levels $\Delta_i, i \geqslant 3$ are fixed to values listed in Table I. See text for details.

w_D (–)	w_1 (–)	θ_D^{LT} (K)	θ_D^{HT} (K)	$\theta_E^{(1)}$ (K)	$\theta_E^{(2)}$ (K)	Δ_1 (K)	Δ_2 (K)	α_{-2}^* (mJ K/mol)	γ_1^* [mJ/(K^2 mol)]	$B_{3/2}^*$ [mJ/(K$^{5/2}$ mol)]
0.21	0.56	504	656	214	526	79	128	9	1.8	0.6

by[53,54]

$$\Delta_2 = \left\{\left(\Delta_2^{(0)}\right)^2 + [2\mu_{\text{eff}}(H_{\text{ex}} + H)]^2\right\}^{1/2}. \qquad (16)$$

Here it is assumed that the molecular exchange field H_{ex} is zero in the antiferromagnetic $PrMnO_3$. Setting the external field $H = 0$, the shift yields $H_{\text{ex}} = 35$ T for $\mu_{\text{eff}} = 1.33\,\mu_B$ (determined from specific heat data[54]) or $H_{\text{ex}} = 27$ T for $\mu_{\text{eff}} = 2.1\,\mu_B$ (as derived from magnetization data).[53] Even though this procedure has to be considered a crude estimate, the values appear to be of the correct order of magnitude. Clearly, they assert a sizable magnetic Pr-Mn exchange in this ferromagnetic and metallic system.

The excess specific heat $C_{\text{exc}}(T)$ was obtained from the difference between the experimental data and the fit [cf. Fig. 9(a)] and associated with the magnetic ordering transition is plotted for data around $T_C = 301$ K in Fig. 11(a). The cusp-like feature should obey the power law of Eq. (1), assuming a continuous phase transition. A fit is possible by considering a constant background term for the nonsingular part of C_p. Determination of the critical exponent α by fitting all parameters in Eq. (1) proved to be instable or produced an exponent close to zero with large uncertainties, depending on the chosen temperature range. Therefore, the exponent was fixed to the expected value for isotropic conventional magnets belonging to the Heisenberg universality class, $\alpha = -0.133$. Omitting the data in the rounded peak region ($300 \leqslant T \leqslant 302$ K), a reasonable fit could be performed and is stable in the temperature range from 290 to 308 K that corresponds to a reduced temperature range of $|\epsilon| \leqslant 0.06$. The critical temperature is determined as $T_C = 302.1 \pm 0.1$. The amplitude ratio [cf. with respect to Eq. (1)] $A^+/A^- = 1.504 \pm 0.015$ is in rather good agreement with the expected universal ratio for Heisenberg-like isotropic magnets $A^+/A^- = 1.56$.[35] This result is in close agreement with an estimate from the anomaly in the temperature derivative of the resistivity $d\rho/dT$ using the Fisher-Langer relation.[6]

From the total excess entropy $C_{\text{exc}}(T)$ the entropy change associated with the magnetic transition has been determined by $S_{\text{exc}}(T) = \int_{T_0}^{T} [C_{\text{exc}}(T')/T']\,dT'$ (with $T_0 = 185$ K) as shown in Fig. 11(b). At 350 K above the transition, $S_{\text{exc}} = 3.16$ J/(mol K). The additional magnetic contribution due to the spin waves is 2.8 J/(mol K) at 350 K, with the $B_{3/2}$ value from Table II. The sum of both magnetic entropy contributions, $S_{\text{mag}} = S_{\text{sw}} + S_{\text{exc}} = 5.97$ J/(mol K), is only about one half of the expected entropy change 12.639 J/(mol K) for a mixed-valent system with $S_1 = 3/2$ and $S_2 = 2$ electronic spins of the Mn ions. This deficiency in discernible magnetic entropy is a common result that has been observed for various ferromagnetic mixed-valent manganites.[39,57,58] If there is no persistence of some magnetic short-range order well above T_C (i.e., the transition is complete at 350 K) then the missing entropy has to be associated with a structural or electronic contribution, for example, a sizable fraction of the lattice specific heat should rely on the magnetic order. However, there is no indication in our data for such an explanation to apply. The most appealing assertion of the missing entropy was proposed by Ramirez *et al.* who argue that the localization of the itinerant electrons through the metal-insulator transition near T_C counterbalances the gain of entropy acquired by the transition into the paramagnetic state.[57] The existence of correlated magnetic polarons is one possible picture that would be consistent with such an electronic mechanism,[59] providing a finite magnetic correlation length. Within this

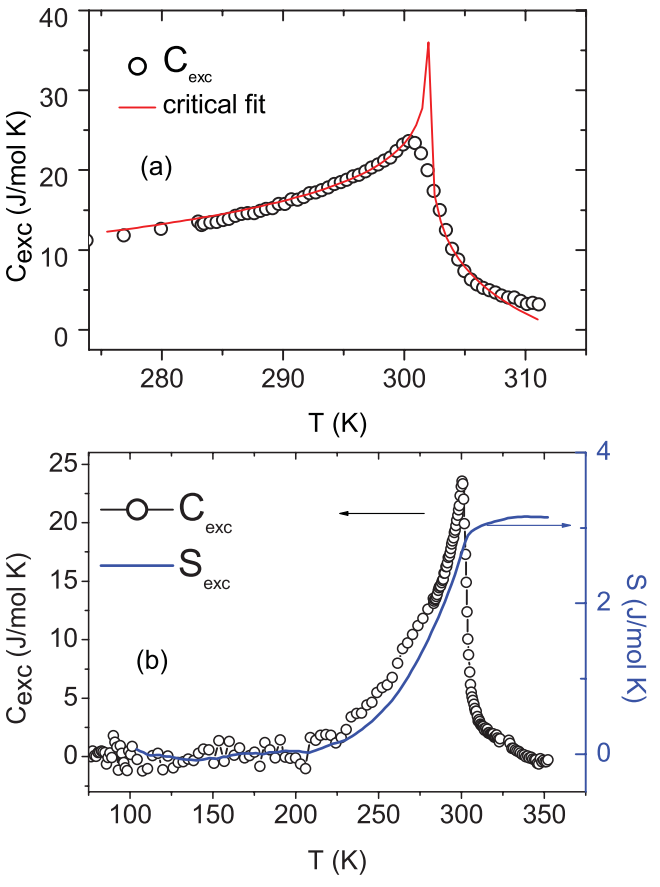

FIG. 11. (Color online) (a) Magnetic specific heat C_{exc}, the solid line is the corresponding power-law fit explained in the text. (b) The excess specific heat at the magnetic transition and the estimated entropy.

picture, measured magnetic entropy data allow us to estimate the size of polaronic entities without any recourse of the microscopic mechanism for their formation by using the assumption that a polaron occupies P sites and has a net moment that is essentially independent of temperature through the ordering transition. The magnetic entropy at the ordering transition of these polarons can be estimated as

$$S^{(d)}_{\mathrm{mag}}(P) = R\big(x \ln\{2\,[S_1 + (P-1)S_2]\} + (1 - xP)\ln(2\,S_2 + 1)\big) \quad \text{for } 1 \leqslant P < 1/x, \tag{17}$$

$$S^{(L)}_{\mathrm{mag}}(P) = (R/P)\ln\{2\,[xS_1 + (1-x)S_2] + 1\} \quad \text{for } P \geqslant 1/x\,. \tag{18}$$

The first case [Eq. (17)] describes a dilute limit of polarons where one hole is delocalized over a few sites. At higher densities $P > 1/x$, larger polarons form a dense assembly filling the whole volume of the material. This is the second case [Eq. (18)] assuming an average spin and local charge neutrality of these larger entities. The measured strong reduction of the entropy, $S_{\mathrm{mag}}/S^{(d)}_{\mathrm{mag}}(P = 1) = 4.7$, at the magnetic ordering means that the system has to be described by the entropy for a dense system of polarons $S^{(L)}$ with average size of $P = 3.7$ sites ($x = 0.4$). This truly microscopic length scale of the magnetic correlations is consistent with the observed universality of a conventional magnetic phase transition in $Pr_{0.6}Sr_{0.4}MnO_3$ but also with a polaronic mechanism for the CMR behavior.

IV. CONCLUSIONS

The ferromagnetic manganite $Pr_{0.6}Sr_{0.4}MnO_3$ with $T_c \sim 301$ K is shown from critical analysis of static magnetization data to behave as a conventional magnetic systems belonging to the 3D Heisenberg universality class. The magnetic anisotropy is not strong enough to drive the system to the 3D Ising universality class, although it influences the scaling analysis. Excellent scaling was achieved for this magnetically complex material such that it can be regarded as a prototype for anisotropic effects in scaling analysis. This metallic system also displays a corresponding critical behavior in resistivity[6] and in the specific heat. The critical analysis of the latter confirms the conventional nature of the magnetic transition in this system. The analysis of the specific heat reveals the presence of a small electronic term associated with the free carriers in the metallic state at low temperatures. At intermediate temperatures, a Schottky-like contribution due to the Pr^{3+} is demonstrated. This contribution in Pr-based metallic mixed-valence systems has not been observed so far, because it is shifted by a Pr-Mn exchange field if compared to the pure $PrMnO_3$ antiferromagnet.

ACKNOWLEDGMENTS

S.R. is thankful to A. Salazar for useful discussions. H.S.N. is grateful to the MPI CPfS for financial support and hospitality in Dresden. The authors thank the Department of Science and Technology, India for financial supports. This work is supported by DAAD-DST exchange program (Pojekt ID 50726385).

*roessler@cpfs.mpg.de

[1] M. B. Salamon and M. Jaime, Rev. Mod. Phys. **73**, 583 (2001).
[2] E. Dagotto, *Nanoscale Phase Separation and Colossal Magnetoresistance: The Physics of Manganites and Related Compounds* (Springer, Berlin, 2003).
[3] Y. Tokura, Rep. Prog. Phys. **69**, 797 (2006).
[4] K. Knížek, Z. Jirák, E. Pollert, F. Zounová, and S. Vratislav, J. Solid State Chem. **100**, 292 (1992).
[5] C. Ritter, P. G. Radaelli, M. R. Lees, J. Baratt, G. Balakrishnan, and D. M. Paul, J. Solid State Chem. **127**, 276 (1996).
[6] S. Rößler, S. Harikrishnan, C. M. N. Kumar, H. L. Bhat, S. Elizabeth, U. K. Rößler, F. Steglich, and S. Wirth, J. Supercond. Nov. Magn. **22**, 205 (2009).
[7] K. Waku, T. Suzuki, T. Nomura, and T. Katsufuji, Phys. Rev. B **72**, 012418 (2005).
[8] R. H. Heffner, L. P. Le, M. F. Hundley, J. J. Neumeier, G. M. Luke, K. Kojima, B. Nachumi, Y. J. Uemura, D. E. MacLaughlin, and S. W. Cheong, Phys. Rev. Lett. **77**, 1869 (1996).
[9] S. E. Lofland, V. Ray, P. H. Kim, S. M. Bhagat, M. A. Manheimer, and S. D. Tyagi, Phys. Rev. B **55**, 2749 (1997).
[10] L. Vasiliu-Doloc, J. W. Lynn, Y. M. Mukhovskii, A. A. Arsenov, and D. A. Shulyatev, J. Appl. Phys. **83**, 7342 (1998).
[11] K. Ghosh, C. J. Lobb, R. L. Greene, S. G. Karabashev, D. A. Shulyatev, A. A. Arsenov, and Y. Mukovskii, Phys. Rev. Lett. **81**, 4740 (1998).
[12] C. V. Mohan, M. Seeger, H. Kronmüller, P. Murugaraj, and J. Ma, J. Magn. Magn. Mater. **183**, 348 (1998).
[13] N. Moutis, I. Panagiotopoulos, M. Pissas, and D. Niarchos, Phys. Rev. B **59**, 1129 (1999).
[14] M. Sahana, U. K. Rößler, N. Ghosh, S. Elizabeth, H. L. Bhat, K. Dörr, D. Eckert, M. Wolf, and K. H. Müller, Phys. Rev. B **68**, 144408 (2003).
[15] S. Nair, A. Banerjee, A. V. Narlikar, D. Prabhakaran, and A. T. Boothroyd, Phys. Rev. B **68**, 132404 (2003).
[16] A. Oleaga, A. Salazar, D. Prabhakaran, and A. T. Boothroyd, Phys. Rev. B **70**, 184402 (2004).
[17] B. Padmanabhan, H. L. Bhat, S. Elizabeth, S. Rößler, U. K. Rößler, K. Dörr, and K. H. Müller, Phys. Rev. B **75**, 024419 (2007).
[18] J. Yang and Y. P. Lee, Appl. Phys. Lett. **91**, 142512 (2007).
[19] J. Yang, Y. P. Lee, and Y. Li, Phys. Rev. B **76**, 054442 (2007).
[20] A. Gamzatov, K. Khizriev, A. Batdalov, S. Abdulvagidov, A. Aliev, O. Melnikov, and O. Gorbenko, Low Temp. Phys. **35**, 214 (2009).
[21] A. K. Pramanik and A. Banerjee, Phys. Rev. B **79**, 214426 (2009).
[22] P. Sarkar, S. Arumugam, P. Mandal, A. Murugeswari, R. Thiyagarajan, S. Esaki Muthu, D. Mohan Radheep, C. Ganguli, K. Matsubayshi, and Y. Uwatoko, Phys. Rev. Lett. **103**, 57205 (2009).
[23] J. Fan, L. Ling, B. Hong, L. Zhang, L. Pi, and Y. Zhang, Phys. Rev. B **81**, 144426 (2010).

[24] Y. Bitla, S. Kaul, L. Fernández Barquín, J. Gutiérrez, J. Barandiarán, and A. Peña, New J. Phys. **12**, 093039 (2010).
[25] A. G. Gamzatov, A. M. Aliev, K. Sh. Khizriev, I. K. Kamilov, and A. S. Mankevich, J. Alloys Compd. **509**, 8295 (2011).
[26] H. S. Shin, J. E. Lee, Y. S. Nam, H. L. Ju, and C. W. Park, Solid State Commun. **118**, 377 (2001).
[27] C. Şen, G. Alvarez, and E. Dagotto, Phys. Rev. Lett. **105**, 97203 (2010).
[28] J. Fan, L. Pi, L. Zhang, W. Tong, L. Ling, B. Hong, Y. Shi, W. Zhang, L. Du, and Y. Zhang, Appl. Phys. Lett. **98**, 072508 (2011).
[29] H. E. Stanley, *Introduction to Phase Transitions and Critical Phenomena* (Oxford University Press, New York, 1971).
[30] H. M. Rietveld, Acta Crystallogr. **22**, 151 (1967).
[31] J. R. Carvajal, Physica B **192**, 55 (1993).
[32] W. Boujelben, M. Ellouze, A. Cheikh-Pouhou, J. Pierre, Q. Cai, W. B. Yelon, K. Shimizu, and C. Bubourdieu, J. Alloys Compd. **334**, 1 (2002).
[33] B. Widom, J. Chem. Phys. **43**, 3898 (1965).
[34] B. Widom, J. Chem. Phys. **41**, 1633 (1964).
[35] M. Campostrini, M. Hasenbusch, A. Pelissetto, P. Rossi, and E. Vicari, Phys. Rev. B **65**, 144520 (2002).
[36] M. Seeger, S. N. Kaul, H. Kronmüller, and R. Reisser, Phys. Rev. B **51**, 12585 (1995).
[37] C. Şen, G. Alvarez, and E. Dagotto, Phys. Rev. Lett. **98**, 127202 (2007).
[38] Y. Tomioka and Y. Tokura, Phys. Rev. B **66**, 104416 (2002).
[39] M. R. Lees, O. A. Petrenko, G. Balakrishnan, and D. M. Paul, Phys. Rev. B **59**, 1298 (1999).
[40] A. K. Raychaudhuri, A. Guha, I. Das, R. Rawat, and C. N. R. Rao, Phys. Rev. B **64**, 165111 (2001).
[41] S. Jandl, V. Nekvasil, A. A. Mukhin, and M. L. Sadowski, J. Magn. Magn. Mater. **311**, 583 (2007).
[42] B. F. Woodfield, M. L. Wilson, and J. M. Byers, Phys. Rev. Lett. **78**, 3201 (1997).
[43] H. Y. Hwang, P. Dai, S. W. Cheong, G. Aeppli, D. A. Tennant, and H. A. Mook, Phys. Rev. Lett. **80**, 1316 (1998).
[44] J. Zhang, F. Ye, H. Sha, P. Dai, J. A. Fernandez-Baca, and E. W. Plummer, J. Phys. Condens. Mater **19**, 315204 (2007).
[45] C. Kittel, *Quantum Theory of Solids* (Wiley, New York, 1954).
[46] W. E. Pickett and D. J. Singh, Phys. Rev. B **53**, 1146 (1996).
[47] A. Podlesnyak, S. Rosenkranz, F. Fauth, W. Marti, H. J. Scheel, and A. Furrer, J. Phys. Condens. Mater **6**, 4099 (1994).
[48] S. Rosenkranz *et al.*, Phys. Rev. B **60**, 14857 (1999).
[49] A. Senyshyn, W. Schnelle, L. Vasylechko, H. Ehrenberg, and M. Berkowski, J. Phys. Condens. Mater **19**, 156214 (2007).
[50] V. Hardy, A. Wahl, C. Martin, and C. Simon, Phys. Rev. B **63**, 224403 (2001).
[51] A. Banerjee, R. Rawat, K. Mukherjee, and P. Chaddah, Phys. Rev. B **79**, 212403 (2009).
[52] A. Wahl, V. Hardy, C. Martin, and C. Simon, Eur. Phys. J. B **26**, 135 (2002).
[53] J. Hemberger, M. Brando, R. Wehn, V. Y. Ivanov, A. A. Mukhin, A. M. Balbashov, and A. Loidl, Phys. Rev. B **69**, 064418 (2004).
[54] J. Cheng, Y. Sui, X. Wang, Z. Liu, J. Miao, X. Huang, Z. Lu, Z. Qian, and W. Su, J. Phys. Condens. Mater **17**, 5869 (2005).
[55] D. Varshney and N. Kaurav, Eur. Phys. J. B **37**, 301 (2003).
[56] N. Ghosh, S. Elizabeth, H. L. Bhat, U. K. Rößler, K. Nenkov, S. Rößler, K. Dörr, and K. H. Müller, Phys. Rev. B **70**, 184436 (2004).
[57] A. P. Ramirez, P. Schiffer, S. W. Cheong, C. H. Chen, W. Bao, T. T. M. Palstra, P. L. Gammel, D. J. Bishop, and B. Zegarski, Phys. Rev. Lett. **76**, 3188 (1996).
[58] J. E. Gordon, R. A. Fisher, Y. X. Jia, N. E. Phillips, S. F. Reklis, D. A. Wright, and A. Zettl, J. Magn. Magn. Mater. **177**, 856 (1998).
[59] C. M. Varma, Phys. Rev. B **54**, 7328 (1996).